Biogeosciences Discuss., 8, 3739–3770, 2011
www.biogeosciences-discuss.net/8/3739/2011/
doi:10.5194/bgd-8-3739-2011


Biogeosciences Discussions



# Environmental factors associated with long-term changes in chlorophyll-*a* concentration in the Amazon floodplain

**E. Alcântara[1], E. M. Novo[1], C. F. Barbosa[2], M.-P. Bonnet[3], J. Stech[1], and J. P. Ometto[4]**

[1]Brazilian Institute for Space Research, Remote Sensing Division, São José dos Campos, SP – Brazil
[2]Brazilian Institute for Space Research, Imaging Processing Division, São José dos Campos, SP – Brazil
[3]Université de Toulouse, UPS (OMP), IRD, LMTG, Toulouse, France
[4]Brazilian Institute for Space Research, Earth System Science Centre, São José dos Campos, SP – Brazil

Received: 29 March 2011 – Accepted: 5 April 2011 – Published: 12 April 2011

Correspondence to: E. Alcântara (enner@dsr.inpe.br)

Published by Copernicus Publications on behalf of the European Geosciences Union.







## Abstract

Long-term environmental time series of continuously collected data are fundamental to identify and classify pulses and determine their role in aquatic systems. This paper presents in situ daily mean chlorophyll-*a* concentration time series, key information for the current understanding of carbon fluxes in and out of the Amazonian floodplain system. This paper also investigates how seasonal fluctuations in water level affect the relationship between chlorophyll-*a* concentration and some of its controlling limnological (water level, water surface temperature, pH and turbidity) and meteorological (wind intensity, relative humidity and short wave radiation) variables provided by an automatic monitoring system (Integrated System for Environmental Monitoring-SIMA) deployed at Curai Lake. The data are collected in preprogrammed time interval (1 h) and are transmitted by satellite in quasi-real time for any user in a range of 2500 km from the acquisition point. We used Pearson correlation to determine the quantitative relationship between chlorophyll-*a* time series and others environmental parameters. Fourier power spectrum analyses were applied to identify periods of high variability in chlorophyll-*a* time series and wavelet power spectrum analyses helped to characterize their time-frequency structure. To further investigate the relationship between chlorophyll-*a* and the statistically significant variable highlighted by Pearson's correlation, the set of time series was submitted to cross wavelet analysis. The time series of chlorophyll-*a* shows two high peaks (47 $\mu g\,L^{-1}$ and 53.30 $\mu g\,L^{-1}$) of concentration during a year: first during the rising water and second during the low water level. A small peak was observed during the high water level (10 $\mu g\,L^{-1}$). For the most part of rising, high and receding water level, the chlorophyll-*a* concentration is often low (from 2.20 $\mu g\,L^{-1}$ to 9.10 $\mu g\,L^{-1}$). chlorophyll-*a* concentration displays periodicities ranging from 2–60 days, with a coherence of approximately 1 in phase with water level during the rising and low water period. Water level dynamics and turbidity explain 68% of the chlorophyll-*a* time series variability.





BGD

8, 3739–3770, 2011



## 1 Introduction

In addition to its importance for the photosynthesis, chlorophyll-*a* is probably the most-often used estimator of algal biomass in inland waters (Melack and Forsberg, 2001) and also one of the easiest measured.

There are many factors affecting the variability of chlorophyll-*a* concentration such as light availability (Kirk, 1994), nutrient (Hecky and Kilham, 1988), zooplankton grazing (Timms and Moss, 1984), thermal structure (Rink et al., 2010) and hydrodynamic (Carrick et al., 1993). Light availability and nutrients, however, are recognized as limiting factors to phytoplankton growth (Carpenter et al., 1999). The present study will focus therefore in improve the understanding of those factors measurable by sensors deployed in a monitoring system.

The study of chlorophyll-*a* concentration in most of the aquatic environments has been based primarily on datasets obtained at different sites or along track lines in cruises (Jerosch et al., 2006). The determination of different scales of temporal variability of biological and environmental parameters is a requirement for any basic ecological study. However, sampling efforts must be carefully considered since misleading conclusions may arise from less intensive data collection, while large sampling programs considerably increase the costs of data acquisition (Alcântara et al., 2008, 2009).

Long-term environmental time series of continuously collected data are fundamental to identify and classify pulses and determine their role in aquatic systems. These pulses can be natural or induced for antropic activity, frequent, seasonal or intermittent, with variable magnitude and both direct and indirect effect (Tundisi et al., 2004). Comprehension of functions and characterization of controlling factors, however, normally arise after the collection of large data sets at different time scales, which allows one to identify and differentiate short and long-term variability.

Some authors have used satellite imagery to address the wide range of spatial and temporal variability of chlorophyll-*a* concentration in the Brazilian Amazon floodplain (Novo et al., 2006). However, the authors have estimated the chlorophyll-*a*





BGD
8, 3739–3770, 2011



concentration in a synoptic view. Also, those studies do not explore the relationship between the chlorophyll-*a* concentration and other environmental parameters that might explain the reported time and space variability.

Based on this, the objective of this study is to describe the temporal variability of chlorophyll-*a* concentration as a function of the flood-pulse variation, using data collected by a moored system. The study also explores the relationship between chlorophyll-*a* time series variability and the time variability of some variables which might affect also its concentration. This study may as well contribute to a better understanding of the carbon fluxes exchanges between Amazon River and floodplain lakes.

## 2 Study site and background

This floodplain, located 850 km from the Atlantic Ocean (Fig. 1), near Óbidos city (Pará State, Brazil), is formed by "white" water lakes characterized by high concentration of suspended sediments, 'black' water lakes with high concentration of dissolved organic matter and low concentration of sediments and "clear" water lakes fed by rainfall and rivers draining from the surrounding "Terra Firme" (Novo et al., 2006; Melack, 1984; Engle and Sarnelle, 1990; Martinez and Le-Toan, 2006). During rising water, sediment-rich river water (white water) inundates the floodplain and directly enters many of the lakes (Forsberg, 1988). During low water, when the lakes are shallower and often isolated from mainstem influence, sediment resuspension can also produce high levels of inorganic turbidity (Junk, 1997).

Based on data acquired from 2001–2002, Bonnet et al. (2008) showed that Curuai lake is filled by water of different sources. In early January (over the course of the 2001–2002 water year), the Amazon River dominated the mixture (64%). From this date until the beginning of April, the river water contribution slightly decreased while contributions from watersheds and direct rainfall increased. By mid-April water from rainfall constituted as much as 17% while contributions from local upland watershed and from watershed located in the aquatic-terrestrial transition zone reached their maxima by the





BGD
8, 3739–3770, 2011



end of February, constituted 14% and 15%, respectively. The groundwater reservoir contribution was highest at the end of December reaching 5% of the mixture (Bonnet et al., 2008).

The residence time of the riverine water within the floodplain is $5 \pm 0.8$ month, while the residence time of water from all sources is $3 \pm 0.2$ months. The lowest and highest absolute water levels recorded at the Curuai gauging station during the 1982–2003 period were 3.03 m and 9.61 m, respectively.

## 3 Methodological approach

### 3.1 Data acquisition

The in situ data was collected from 2004 to 2007 by an autonomous system called "SIMA" (Integrated System for Environmental Monitoring). SIMA is a set of hardware and software designed for data acquisition and real time monitoring of hydrological systems (Stech et al., 2006). Its is composed of an independent system formed by an anchored buoy, in which sensors, data storage systems, battery and the transmission antenna are fixed (Fig. 2).

The data are collected in preprogrammed time interval (1 h) and are transmitted by satellite in quasi-real time for any user in a range of 2500 km from the acquisition point. In this study the following environmental parameters chlorophyll-*a* ($\mu g\,L^{-1}$), turbidity (NTU), water level (m), wind intensity ($ms^{-1}$), relative humidity (%), short wave radiation ($Wm^{-2}$) water surface temperature (°C), water column temperature by a thermistor string (°C) and pH were used. The characteristics of the sensors are show in Table 1.

### 3.2 Data processing

In order to overcome the problem of missing data in the time series two approaches were applied: first a simple moving average technique was used to fill small gaps (Box





BGD
8, 3739–3770, 2011



and Jenkins, 1994); second, during long spells of system malfunctioning, a synthetic series of data was computed by combining and averaging the available data. The synthetic time series can be considered for majority of the observations in the series as a four-year daily mean. The authors are aware that this approach precludes the understanding of the inter-annual variability, but, on the other hand allow the analyses of a continuous series (Hipel and McLeod, 1994).

The water column temperature time series, in four depths (2, 4, 6 and 10 m), was vertically interpolated using a linear function available in Matlab software (The MathWorks Inc.). Considering the lack of nutrient information in the time series, temperature thermal structure was analyzed as a surrogate based on the relationship between water column mixing and nutrient availability (Weitholff et al., 2000).

### 3.3 Data analysis

Pearson correlation was run to determine the quantitative relationship between chlorophyll-*a* time series and meteorological and limnological data (Zar, 1996).

#### 3.3.1 Time series analysis

To analyze the temporal modes of variability of the chlorophyll-*a* time series, we used Fourier Power Spectrum, Wavelet Analysis and Cross Wavelet and Coherence and Phase.

Spectrum analysis deals with the identification of cyclical patterns in the data. Data windowing was used to smooth the power spectrum, thereby reducing its variance and increasing statistical confidence although it may cause spectral leakage (Press et al., 1992; Bloomfield, 2000). To reach a compromise between strong smoothing (more confidence but stronger bias) and weak smoothing (less confidence but less bias) with an acceptable spectral leakage, we generated our power spectrum estimates using a smoothing Hamming window of variable length.





BGD
8, 3739–3770, 2011



The temporal variability of the frequency content of the chlorophyll-*a* concentration time series was analyzed using the Wavelet Transform (Torrence and Compo, 1998). The decomposition of environmental time series into time-frequency space allows for the determination of both the dominant modes of variability and how those modes vary in time. The chlorophyll-*a* time series obtained from SIMA were analyzed by continuous wavelet analysis using the Morlet wavelet (Meyers et al., 1993).

To show the relationship between chlorophyll-*a* and the significantly time series highlighted by Pearson's correlation the cross wavelet analysis was carried out and the coherence and phase analyzed (Maraun and Kurths, 2004). The cross wavelet transform $W^{xy}$ of the two time series $x_n$ and $y_n$ is a complex function. The cross wavelet power spectrum is defined as $\left|W^{xy}\right|$, and its complex argument arg ($W^{xy}$) can be interpreted as the local relative phase between $x_n$ and $y_n$ in the time-frequency space (Torrence and Webster, 1998; Grinsted et al., 2004).

The calculation procedures of Fourier Power Spectrum, Wavelet Power Spectrum and Cross Wavelet and Wavelet Coherence were coded in Matlab 6.5 (The MathWorks, Inc., *Natick, MA*).

## 4 Results and discussion

### 4.1 The thermal structure

The thermal structure obtained by a thermistor string installed in SIMA buoy shows that in Curuai floodplain from January to April and November to December the water column are stratified and from April to October the water column are mixed (Fig. 3). The thickness of the mixing layer starts deepening in December and stop in April when reach approximately 7 m. This is in accordance with Imberger (1985) that defines the surface mixed layer as that part of the water column immediately below the free surface, which is directly influenced surface wind stress and buoyancy flux.





BGD
8, 3739–3770, 2011



Due to location of SIMA buoy in the floodplain (see Fig. 1 for location) the thermistor installed at 2m depth reveals that a cold water are inserted into the floodplain from the Amazon River (rising water level) and by runoff (wet season). When the water level is high and there is no exchange of water between Amazon River and floodplain the water column mixing. According to McIntyre and Melack (1988) local currents resulting from the inflow of river water or affluent from the "Terra Firme" (surrounding higher terrain with no flooding events) can modify the stratification pattern. That might be the case in the region where the SIMA is settled, since it is very close to the "Terra Firme" drowned river mouth or "rias" which makes up the Curuai lake floodplain system (Barbosa et al., 2010).

Mixing depth exerts control over light availability that may in turn affect phytoplankton community structure according to algal sinking velocity and light-dependent growth (Reynolds et al., 2002). The mixing depth is also an important determinant of phytoplankton standing stock and zooplankton biomass within the mixed layer of lakes (Berger et al., 2006).

It is fact that during the stratified period the concentration of chlorophyll-*a* is higher than during the mixing period. The major influence of stratification is the creation of layers with high concentration of nutrients and some specific species of algae, mainly in the metalimnion. The processes of mixing and stratification can affect the selection and vertical distribution of phytoplankton species, since they affect the availability of essential resources. During the low water level, where there is low-light availability and high nutrient concentration, probably the cryptophytes are dominant (Ptacnik et al., 2003); during the rising water level, where the light availability is higher than low water level period, and the thermocline is deeper, the diatoms and cyanophytes can be dominants (Reynolds, 1984).

### 4.2 The time series

A general analysis of the chlorophyll-*a* concentration time series shows two outstanding peaks: the first during January–February (a) and the second during





BGD
8, 3739–3770, 2011



October–November (b) while concentration remains low from March–September (c) and in December (Fig. 4). This high chlorophyll-*a* concentration during low water level was also observed in the Central Amazonian floodplain lake (Ibãnez, 1998).

The turbidity time series has a large peak from October to November (d), a small peak from January to February (e) and remains relatively low all the rest of the year (f) except a peak in August (g). Note that chlorophyll-*a* concentration and turbidity time series have quasi-same peaks and that these peaks occur during rising (a, e) and low water level (b, d). The wind intensity is higher from March to August (h) than from September to November (i).

The relative humidity has two peaks, first in the beginning of the hydrological year (j) and second in the end (k); also a decrease in August-September (l) when the short-wave radiation is shutting down (m). The water surface temperature presents three main features, the first from January to March (n) with temperature between 24–29°C, the second from April to July (o) with temperature ranging from 24 to 27°C and the third from August to December (p) ranges from 26–31°C.

The pH has a relatively small variability through the time, with just some interesting events, one in August and September (q) when the pH is below 7 and in November (r) when the value rises up to ~8.8.

The descriptive statistics (maximum, minimum, mean and standard deviation) of these time series is show in Table 2.

The time dependence of the chlorophyll-*a* concentration could be accessed using a fitting function. The time series of chlorophyll-*a* was adjusted using eight Gaussian-terms. Due to the high variability observed by the end of January and by October-November (Fig. 5a) the model did not capture all the variability.

Where (h) is the amplitude, (t) time, ($\mu$) the central or peak position and ($\sigma$) the variance.

This is observed in Fig. 5b which shows the highest residuals during this period (i and ii, respectively). From August to May and from July to September the model fitted very well. The overall fitting was $R^2 = 0.94$ ($p = 0.05$ and RMSE = 1.96). The Table 3





BGD
8, 3739–3770, 2011



summarizes the time-frame explained by each of the terms. All this variability could be addressed using the Fourier and Wavelet analysis.

The Fourier power spectrum applied to chlorophyll-*a* time series shows that the power density increases with time in four major peaks, the first in 6 days (a), second in 18 days (b), third in 30 days (c) and in 46 days (d), see Fig. 6. Also we observe a continuously increasing power density in 55 days.

The period of 6 days means that in short periods of days the chlorophyll-*a* can change rapidly and stay associated with the two major peaks (beginning of January and October–November) presented above in Fig. 5. The periods of 18 days is associated, probably, with the two peaks presented in Fig. 5 from October–November. Periods higher than 30 days are associated with relatively small peaks in half of June and the end of November. For a more detailed evaluation about these periods a wavelet transform was run.

The wavelet power spectrum (Fig. 7) reveals that the highest energy occurs from January to February (a) and from October to December (b). During January the band periods of this higher energy ranges from 2–32 days. That is, when the Amazon waters enters into the Curuai floodplain the chlorophyll-*a* concentration change rapidly (2 days) and keep increasing throughout the month.

When the water level is high the variations in concentration can occur with high energy for periods larger than a month (c) and with low energy for periods ranging from 2 to 22 days (d). With the water exchange from the floodplain to the Amazon River the chlorophyll-*a* concentration can change dramatically again in periods less than 5 days (e). This is more pronounced during the low water level in November and December (b). During the low water level the periods of high variability in chlorophyll concentration can vary from 2 days to 2 months.

The influence of others environmental parameters on chlorophyll-*a* annual variability pattern will be checked using two approaches: (1) Pearson's correlation between the chlorophyll concentration and the others time series, (2) second applied the cross wavelet between the correlated time series.





BGD
8, 3739–3770, 2011



### 4.3 Pearson's correlation

The results of Pearson's correlation (Table 4) shows that the chlorophyll-*a* time series is negatively correlated with water level (−0.57) and positively with turbidity (0.66). That means, when there is an increase in water level the chlorophyll concentration decreases and when chlorophyll concentration increases the turbidity increases. The others parameters show a very low correlation. Because of that, the remaining analyses will focus on those variables displaying high correlation with chlorophyll-*a*.

As indicated in Table 2, the water level is about two times greater during high water level stage than during low water stage and consequently the floodplain volume are varying of about a factor 3. Part of the inverse correlation obtained may therefore be attributed to chlorophyll-*a* dilution.

A negative correlation between water level and chlorophyll-*a* is also expected in turbid environments where phytoplankton has to remain in the euphotic zone. Most of the phytoplankton species tends to sediment and cells are passively transported. The stay-duration in the euphotic zone depends on the water circulation, in particular circular movement such as wave-induced currents or vertical movements that help the cells to remain in the upper part of the water column.

When depth increases, phytoplankton has therefore less chance to maintain in the euphotic zone as reported by (Junk, 1997). However, this control depends on phytoplankton species. In the floodplain occasional blooms of cyanobacteria can occur during part of the year and these species have buoyancy control abilities that help them to remain at the surface (Uherkovich and Schmidt, 1974; Fiore et al., 2005).

As pointed out by Melack and Forsberg (2001) the total daily phytoplankton production can vary considerably in Amazon floodplain lakes due to large seasonal changes in surface area linked to water-level variations. The dependence of productivity on the water level was also reported by Schmidit (1973) where the maximum production per unit volume (2.15 $gCm^{-3}\,day^{-1}$) occur during the low water level and the minimum production was found during the rising water level (0.32 $gCm^{-3}\,day^{-1}$).





BGD
8, 3739–3770, 2011



Although the high turbidity during the low water level, the concentration of chlorophyll-*a* is high. In accordance to Ibãnez (1998) the negative impact of low transparency was counteracted by shallow water depth and additional nutrient input from the sediment, birds, and aquatic macrophytes decomposition.

Seasonal variability of shortwave radiation is very low in the study area compared with other regions of the world. Changes in incoming shortwave radiation are not directly a driving factor for photosynthesis or communities successions, but probably light availability does as mentioned by (Forsberg, 1988). The floodplain alkalinity is relatively medium when compared to the world's river average (Martin and Meybeck, 1979), strong primary production and/or respiration activities should therefore lead to significant pH changes during the day which are lost by using daily-averaged values.

The water level dynamics and turbidity explain 68% of the chlorophyll-*a* time series variability (RMS = 11.27 $\mu g\,L^{-1}$, $\rho = 0.04$) and could be represented as:

$$Chl = 23.01 - (0.20WL) - (0.50Tur) \quad (1)$$

This statistical model was evaluated through the use of a separated set of chlorophyll-*a* concentration derived from the SIMA buoy (Fig. 8). The figure shows three band of concentration that deserves attention: (a) chlorophyll-*a* concentration from 30 to 60 $\mu gL^{-1}$ underestimated; (b) concentration bellow 10 $\mu g\,L^{-1}$ is overestimated and (c) for concentration from 4 to 19 $\mu g\,L^{-1}$ the model fits well.

The evaluation shows that the statistical model (Eq. 2) presents their better results for concentrations measured during the rising, high and receding water level. For concentrations measured during the low water level the model fail. The causes of the poor results for the low water period are due to high dynamic and variable concentrations encountered during this phase (see Fig. 5). As shown in Fig. 4 during the low water level the chlorophyll-*a* concentration and the turbidity is very high.

The time frequency structure between chlorophyll-*a* and turbidity and water level will be analyzed in more detail using the cross wavelet spectrum analyses. Taking into account that only water level and turbidity showed significant correlations with chlorophyll, from now on, the cross correlation analyses will be focused upon them.





BGD
8, 3739–3770, 2011



### 4.4 Cross wavelet and coherence and phase analyses

Cross wavelet power reveals areas with high common power between two parameters and coherence is a measure of the correlation between two time series, at each frequency. Arrows pointing to the right mean correlation (in phase) and an anticorrelation (in antiphase) is indicated by a left pointing arrow. Non-horizontal arrows refer to a more complicated (non-linear) phase difference (Valdés-Galicia and Velasco, 2008).

The cross wavelet spectrum between chlorophyll and turbidity (Fig. 9a) is stronger at the 2 to 30 day band (i) and occurs during the low water level, when the turbidity is very high. The same band period occurs at the beginning of the time series but displaying medium power (ii) when the Amazon water entering the floodplain.

The coherence (Fig. 9b) is more highlighted from 3 to 50-days (iii) band (in-phase) in the beginning of the time series and from 2 to 16-days band periods (in-phase) in the end of the time series (iv). Moreover the coherence is stronger for 32-days in the beginning and 16-days and periods for the end of time series.

For chlorophyll-*a* and water level the cross wavelet spectrum (Fig. 9c) shows a significant period 64–94 days (v) band (in-phase) during the receding water level. That is, when the water is exchanged from floodplain to Amazon River. For periods smaller than 64 days the water level is not a determinant variable to cause algal bloom. However from September to February the water level is very important. The coherence (Fig. 8e) shows an increase of period for high coherence (vi). Suggesting that from September to December the water level dynamics is more important than in January and February.

The positive correlation between turbidity and chlorophyll-*a* and high pH during the largest peak in October–November confirms that there is a strong production during that period of time while turbidity is high.

The short-time response observed in December–January and August–November (Fig. 5) is related to higher values of chlorophyll-*a* concentration observed in Fig. 5a. During the peak observed in August–November when the water level is lowering, there





BGD
8, 3739–3770, 2011



are sediment re-suspension events, as reported by (Alcântara et al., 2010). When this event occurs nutrients are made available to the water column, as reported by (Forsberg et al., 1988) and supported by (Engle and Sarnelle, 1990; Carpenter, Ludwig and Brock, 1999).

Ibañez (1998) also reported for a central Amazonian floodplain, that during the rising and low water level phytoplankton species richness is higher than receding and high water level. In the case of December–January is related to incoming water from Amazon River into floodplain and also by local water basin due to precipitation. The average annual precipitation in the Curuai floodplain is 2447 mm year$^{-1}$, compared to average potential evaporation of 1400 mm year$^{-1}$ (average obtained by a time series from 1990 to 2001), with the wet season lasting from January to June and a drier season from July to December (Barroux, 2006).

During the high water level sediment accumulates in the floodplain, while during the receding water stage it is exported to the mainstream. The mean average sediment storage calculated for the floodplain varies between 558 and 828 $\times$ 10$^{3}$ t yr$^{-1}$ (Maurice-Bourgoin et al., 2007). According to Moreira-Turcq et al. (2004) the Curuai floodplain is a sediment accumulation system, with high rate of bottom deposition in some specific lakes (i.e. Santa Ninha Lake, 1 cm yr$^{-1}$). Of the influx of suspended material from the Amazon River into the floodplain, about 50% is deposited. Amorim (2006) shows that in general manner the suspended materials in the Curuai floodplain is composed mainly of silt and clay.

Probably, because of this during the high and failing water level the concentration of chlorophyll-*a* in the Curuai floodplain is low. However, in June a short increase in chlorophyll concentration occurs. This is an effect of sediment deposition and consequent increase in light availability; afterward, the concentration stabilizes. This is supported by Forsberg et al. (1988) who have found that during the high water level stage the phytoplankton growth due to high transparency caused by particulate settling.

Then a high phytoplankton growth causes a peak of chlorophyll concentration as shown in Fig. 5 and it is confirmed by high pH values (around 8.8) indicating a strong





BGD
8, 3739–3770, 2011



photosynthesis activity. Immediately afterwards a decrease of chlorophyll concentration occurs. This decrease was captured by the Sixth Gaussian term of the Eq. (1). With high turbidity and high competition for nutrients and solar radiation some cells starts to die, increasing the concentration of dissolved organic matter and decreasing of dissolved oxygen, as shown by (Barbosa et al., 2010).

## 5 Summary and conclusion

The present works is a contribution to understanding the chlorophyll variability through the time. In summary, we have demonstrated that:

The short-time responses are associated with the most significant peaks of chlorophyll-*a* and in particular the shortest time response seems to occur during October and November. The small periods of variability evidenced by Fourier and Wavelet might be related to sediment re-suspension events during low water level that allow also the nutrient availability.

Significant Pearson's correlation between water level (negative), turbidity (positive) and chlorophyll-*a* were obtained. Cross wavelet analysis and coherence study enabled to show a strong influence of water level during the second peak as well as a strong influence of turbidity on short-time responses while during the first peak both water level and turbidity are less significant.

The pattern of stratification and mixing processes in the Curuai floodplain can influence the nutrient paths and availability, consequently the lake productivity.

A detailed study should be done about the algae species composition in the Curuai Lake during the stratification and mixing periods to be possible to obtain in more information about the influence of physical processes on phytoplankton.

*Acknowledgements.* The authors are grateful to the Brazilian funding agency FAPESP under grants 02/09911-1 and the Brazilian Council for Science and Technology (Grant CNPq-CTHIDRO – 55.0301/02-0, Grant CNPq n.° 477885/2007-1). Evlyn Novo thanks CNPq grant 304929/2007 and Enner Alcântara CAPES grant 0258059 and FAPESP 2007/08103-2. We





BGD
8, 3739–3770, 2011



also thank C. Torrence and G. Compo for provides the Wavelet software and to A. Gristed for provides the cross wavelet and wavelet coherence algorithm software.

## References

Alcântara, E., Novo, E., Stech, J., Lorenzzetti, J., Barbosa, C., Assireu, A., and Souza, A.: A contribution to understanding the turbidity behaviour in an Amazon floodplain, Hydrol. Earth Syst. Sci., 14, 351–364, doi:10.5194/hess-14-351-2010, 2010.

Alcântara, E. H., Stech, J. L., Novo, E. M. L. M., Shimabukuro, Y. E., and Barbosa, C. C. F.: Turbidity in the Amazon floodplain assessed through a spatial regression model applied to fraction images derived from MODIS/Terra., IEEE Trans. Geo. Rem. Sens, 46, 2895–2905, 2008.

Alcântara, E. H., Barbosa, C. C. F., Stech, J. L., Novo, E. M. L. M., and Shimabukuro, Y. E.L Improving the spectral unmixing algorithm to map water turbidity distributions, Environ. Model. Soft, 24, 1051–1061, 2009.

Amorim, M. A., Study of early sedimentation in “Lago Grande de Curuai” várzea, Pará State, Brazil. MSc. Dissertation, Fluminense Federal University, Niterói, Brazil, 2006.

Barbosa, C. C. F., Novo, E. M. L. M., Melack, J. M., Gastil-Buhl, M., and Filho, W. P.: Geospatial analysis of spatiotemporal patterns of pH, total suspended sediment and chlorophyll-*a* on the Amazon floodplain, Limnology, 11, 155–166, 2010.

Barroux, G.: Bio-geochemical study of a lake system from the Amazonian floodplain: the case of Lago Grande de Curuai, Pará-Brazil, PhD. Dissertation, Université Paul Sabatier, Toulouse, France, 2006.

Berger, S. A., Diehl, S., Kunz, T. J., Albrecht, D., Oucible, A. M., and Ritzer S.: Light supply, plankton biomass, and seston stoichiometry in a gradient of lake mixing depths, Limnol. Oceanogr., 51, 1898–1905, 2006.

Bloomfield, P.: Fourier analysis of time series: an introduction. John Wiley and Sons: New York, 2000.

Bonnet, M. P., Barroux, G., Martinez, J. M., Seyler, F., Moreira-Turcq, P., Cochonneau, G., Melack, J. M., Boaventura, G., Maurice-Bourgoin, L., León, J. G., Roux, E., Calmant, S., Kosuth, P., Guyot, J. L., and Seyler, P.: Floodplain hydrology in an Amazon floodplain lake (Lago Grande de Curuaí), J. Hydrology, 349, 18–30, 2008.





BGD
8, 3739–3770, 2011



Box, G. E. P. and Jenkins, G. M.: Time Series Analysis: Forecasting and Control, 3rd edition, Prentice Hall, 1994.
Carrick, H. J., Aldridge, F. J., and Schelske, C. L.: Wind influences phytoplankton biomass and composition in a shallow, productive lake, Limnol. Oceanogr., 38, 1179–1192, 1993.
Carpenter, S. R., Ludwig, D., and Brock, W. A.: Management of eutrophication for lakes subject to potentially irreversible change, Ecol. Appl., 9, 751–771, 1999.
Engle, D. L. and Sarnelle, O.: Algal use of sedimentary phosphorus from an Amazon floodplain lake: implications for total phosphorus analysis in turbid waters, Limnol. Oceanogr., 35, 483-490, 1990.
Farge, M.: Wavelet transforms and their applications to turbulence, Ann. Rev. Fluid Mech., 24, 395–457, 1992.
Fiori, M. F., Neilan, B. A., Copp, J. N., Rodrigues, J. L. M., Tsai, S. M., Lee, H., and Trevors, J. T.: Characterization of nitrogen-fixing cyanobacteria in the Brazilian Amazon floodplain, Water Res., 39, 5017–5026, 2005.
Forsberg, B. R., Devol, A. H., Richey, J. E., Martinelli, L. A., and Des Santos, H.: Factors controlling nutrient concentrations in Amazon floodplain lakes, Limnol. Oceanogr., 33, 41–56, 1988.
Grinsted, A., Moore, J. C., and Jevrejeva, S.: Application of the cross wavelet transform and wavelet coherence to geophysical time series, Non. Lin. Proc. Geophy, 11, 561–566, 2004.
Heckey, R. E. and Kilham, P.: Nutrient limitation of phytoplankton in freshwater and marine environments: a review of recent evidence on the effects of enrichment, Limnol. Oceanogr., 33, 796–822, 1988.
Hipel, K. W. and McLeod, A. I.: Time Series Modeling of Water Resources and Environmental Systems, North-Holland, Amsterdam, 1994.
Ibãnez, M. S. R.: Phytoplankton composition and abundance of a central Amazonian floodplain lake, Hydrobiologia, 362, 79–83, 1998.
Imberger, I.: The diurnal mixed layer, Limnol. Oceanogr., 30, 737–770, 1985.
Jerosch, K., Schlüter, M., and Pesch, R.: Spatial analysis of marine categories information using indicator Kriging applied to georeferenced video mosaics of the deep-sea Håkon Mosby Mud Volcano, Ecol. Infor, 1, 391–406, 2006.
Junk, W. J.: The Central Amazon Floodplain: ecology of a pulsing system, 1rd Ed.; Springer Verlag: Berlin, Germany, 1997.
Kirk, J. T. O.: Light and photosynthesis in aquatic ecosystems, 2nd Edition, Cambridge Univer-





BGD
8, 3739–3770, 2011



sity Press: Cambridge, 1994.
Martin, J. M. and Meybeck, M.: Elemental mass balance of material carried by major world rivers, Mar. Chem., 7, 173–206, 1979.
Martinez, J.-M. and Le-Toan, T.: Mapping of flood dynamics and spatial distribution of vegetation in the Amazon floodplain using multitemporal SAR data, Rem. Sens. Envir, 108, 209–223, 2006.
Maurice-Bourgoin, L., Bonnet, M. P., Martinez, J. M., Kosuth, P., Cochonneau, G., Moreira-Turcq, P., Guyot, J. L., Vauchel, P., Filizola, N., and Seyler, P.: Temporal dynamics of water and sediment exchanges between the Curuaí floodplain and the Amazon River, Brazil, J. Hydrology, 335, 140–156, 2007.
Maraun, D. and Kurths, J.: Cross wavelet analysis: significance testing and pitfalls, Non. Lin. Proc. Geophy., 11, 505–514, 2004.
MacIntyre, S. and Melack, J. M.: Frequency and depth of vertical mixing in an Amazon floodplain lake (Lake Calado, Brazil), Verh. Internat. Verein. Limnol, 23, 80–85, 1988.
Meyers, S. D., Kelly, B. G., and O'Brien, J. J.: An introduction to wavelet analysis in Oceanography and Meteorology: with application to the dispersion of Yanai Waves, Mon. Wea. Rev, 121, 2858–2866, 1993.
Melack, J. M.: Amazon floodplain lakes: shape, fetch and stratification, Int. Ver. Theor. Angew. Limnol. Verh, 22, 1278–1282, 1984.
Melack, J. M. and Forsberg, B. R.: Biogechemistry of Amazon floodplain lakes and associated wetlands, in: the biogeochemistry of the Amazon basin, edited by: McCalin, M. E., Victoria, R. L., Richey, J. E., Oxford University Press. Chap., 14, 235–274, 2001.
Moreira-Turcq, P. F., Jouanneau, B., Turcq, B., Seyler, P., Weber, O., and Guyot, J. L.: Carbon sedimentation at Lago Grande de Curuaí, a floodplain lake in the low Amazon region: insight into sedimentation rates, Palae. Palae. Palae, 214, 27–70, 2004.
Novo, E. L. M. M., Barbosa, C. C. F., Freitas, R. M., Shimabukuro, Y. E., Melack, and J. M., Pereira-Filho, W.: Seasonal changes in chlorophyll distribution in Amazon floodplain lakes derived from MODIS images, Limnology, 7, 153–161, 2006.
Ptacnik, R., Diehl, S., and Berger, S.: Performance of sinking and nonsinking phytoplankton taxa in a gradient of mixing depths, Limnol. Oceanogr., 48, 1903–1912, 2003.
Press, W. H., Teukolsky, S. A., Vetterling, W. T., and Flannery, B. P.: Numerical recipes in fortran 77: the art of scientific computing, V.1 of Fortran numerical recipes, Cambridge University Press: UK, 1992.





BGD
8, 3739–3770, 2011



Reynolds, C. S.: The Ecology of Freshwater Phytoplankton. Cambridge, UK: Cambridge University Press, 1984.
Reynolds, C. S., Huszar, V., Kruk, C., Naselli-Flores, L., and Melo, S.: Towards a functional classification of the freshwater phytoplankton, J. Plankton Res., 24, 417–428, 2002.
Rink, K., Yeates, P., and Rothhaupt, K.-O.: A simulation study of the feedback of phytoplankton on thermal structure via light extinction, Freshwater Biology, 55, 1674–1693, 2010.
Schmidt, G. W.: Primary production of phytoplankton in the three types of Amazonian waters, II. The limnology of a tropical flood-plain lake in Central Amazonia (Lago do Castanho), Amazoniana, 4, 139–203, 1973.
Stech, J. L., Lima, I. B. T., Novo, E. M. L. M., Silva, C. M., Assireu, A. T., Lorenzzetti, J. A., Carvalho, J. C., Barbosa, C. C. F., and Rosa, R. R.: Telemetric monitoring system for meteorological and limnological data acquisition, Verh. Internat. Verein, Limnol, 29, 1747–1750, 2006.
Timms, R. M. and Moss, B.: Prevention of growth of potentially dense phytoplankton populations by zooplankton grazing, in the presence of zooplanktivorous fish, in a shallow wetland ecosystem, Limnol. Oceanogr., 29, 472–486, 1984.
Torrence, C. and Compo, G. P.: A Practical Guide to Wavelet Analysis, Bull. Amer. Meteor. Soc, 79, 61–78, 1998.
Torrence, C. and Webster, P.: Interdecadal changes in the ENSO-Monsoon system, J. Climate, 12, 2679–2690, 1999.
Tundisi, J. G., Matsumura-Tundisi, T., Arantes Junior, J. D., Tundisi, J. E. M., Manzini, N. F., and Ducrot, R.: The response of Carlos Botelho (Lobo, Broa) reservoir to the passage of cold fronts as reflected by physical, chemical and biological variables, Braz. J. Bio, 64, 177–186, 2004.
Valdés-Galicia, J. F. and Velasco, V. M.: Variations of mid-term periodicities in solar activity physical phenomena, Adv. Space Res., 41, 297–305, 2008.
Weithoff, G., Lorke, A., and Walz, N.: Effects of water–column mixing on bacteria, phytoplankton, and rotifers under different levels of herbivory in a shallow eutrophic lake, Oecologia, 125, 91–100, 2000.





BGD
8, 3739–3770, 2011



**Table 1.** Characteristics of the limnological and meteorological sensors in SIMA.

| Sensor | Manufacture | Range | Accuracy | Depth/Height |
|---|---|---|---|---|
| chlorophyll-*a* | Yellow Spring | 0–400 µm | 0.1 µm | −1.30 m |
| Water Temperature | Yellow Spring | −5–60 °C | ±0.15 °C | −1.30 m |
| Thermistor String | Yellow Spring | −5–60 °C | ±0.15 °C | −2, −4, −6 e −10 m |
| Turbidity | Yellow Spring | 0–1000 NTU | 0.1 NTU | −1.30 m |
| Wind | R.M. Young | 0–100 $ms^{-1}$ | ±0.3 $ms^{-1}$ | 3 m |
| Humidity | Rotronic | 0–100 % | ±1.5% | 3 m |
| Shortwave | Kipp & Zonen CM21 | 0–1500 $Wm^{-2}$ | ±1–3% | 3 m |





BGD
8, 3739–3770, 2011



**Table 2.** Descriptive statistics for the time series: chlorophyll-*a* (*Chl*), water level (WL), wind intensity (WI), relative humidity (Rh), short wave radiation (SW), water surface temperature (WST), pH and turbidity (Tur).

| Variables | Max | Min | Mean | SD |
|---|---|---|---|---|
| *Chl* | 53.30 | 2.20 | 10.40 | ±9.11 |
| Tur | 913.24 | 5.76 | 133.93 | ±198.92 |
| WL | 10.13 | 4.45 | 7.60 | ±1.95 |
| WI | 5.86 | 0.86 | 2.83 | ±1.04 |
| Rh | 92.31 | 49.02 | 75.95 | ±7.26 |
| SW | 319.30 | 8.33 | 142.16 | ±64.95 |
| pH | 8.34 | 6.20 | 7.28 | ±0.29 |
| WST | 31.12 | 23.73 | 27.72 | ±1.40 |





BGD
8, 3739–3770, 2011



**Table 3.** Summary of the Gaussian terms used to fit the chlorophyll-*a* time series.

| Gaussian terms | Time-frame | Variance ($\mu gL^{-1}$) |
|---|---|---|
| 1 | January | 2.03 |
| 2 | February–August | 22.69 |
| 3 | September–October | 26.29 |
| 4 | Middle of October | 9.16 |
| 5 | End of October | 2.47 |
| 6 | Beginning of November | $1.41 \times 10^5$ |
| 7 | End of November | 4.42 |
| 8 | December | 14.74 |





BGD
8, 3739–3770, 2011



**Table 4.** Pearson correlation coefficients for chlorophyll-*a* (*Chla*) against water level (WL), wind intensity (WI), relative humidity (Rh), short wave radiation (SW), water surface temperature (WST), pH and turbidity (Tur).

| *Variables* | *r* |
|---|---|
| Tur | 0.66 |
| WL | −0.57 |
| Rh | 0.26 |
| WI | −0.26 |
| WST | −0.16 |
| SW | – |
| pH | – |

Only significant values at 95% significance level are shown.





BGD
8, 3739–3770, 2011



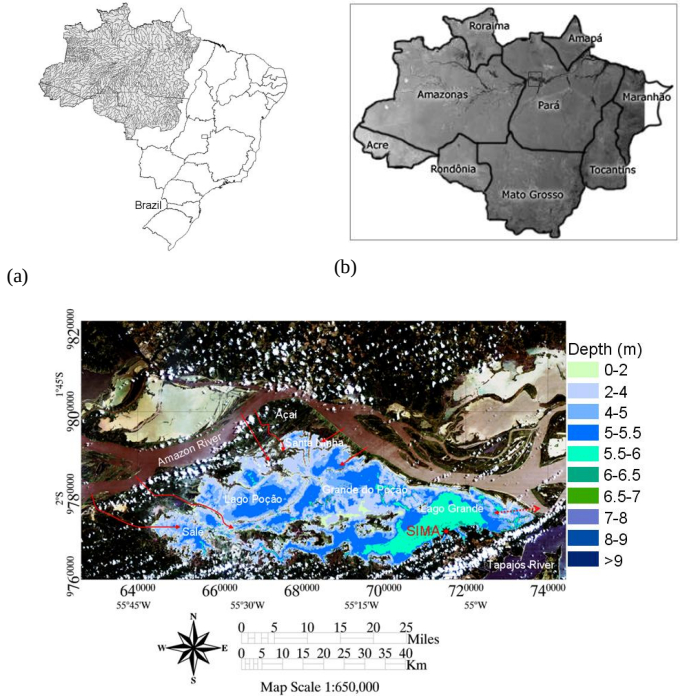


**Fig. 1.** **(a)** Location of Legal Amazon in Brazil, **(b)** Legal Amazon limits, and **(c)** Location of Curuai Floodplain (Pará State, Brazil) and the location of the automatic environmental data collection buoy system SIMA at "Lago Grande". The arrows indicate the main channels of connection Amazon River-floodplain.





BGD
8, 3739–3770, 2011



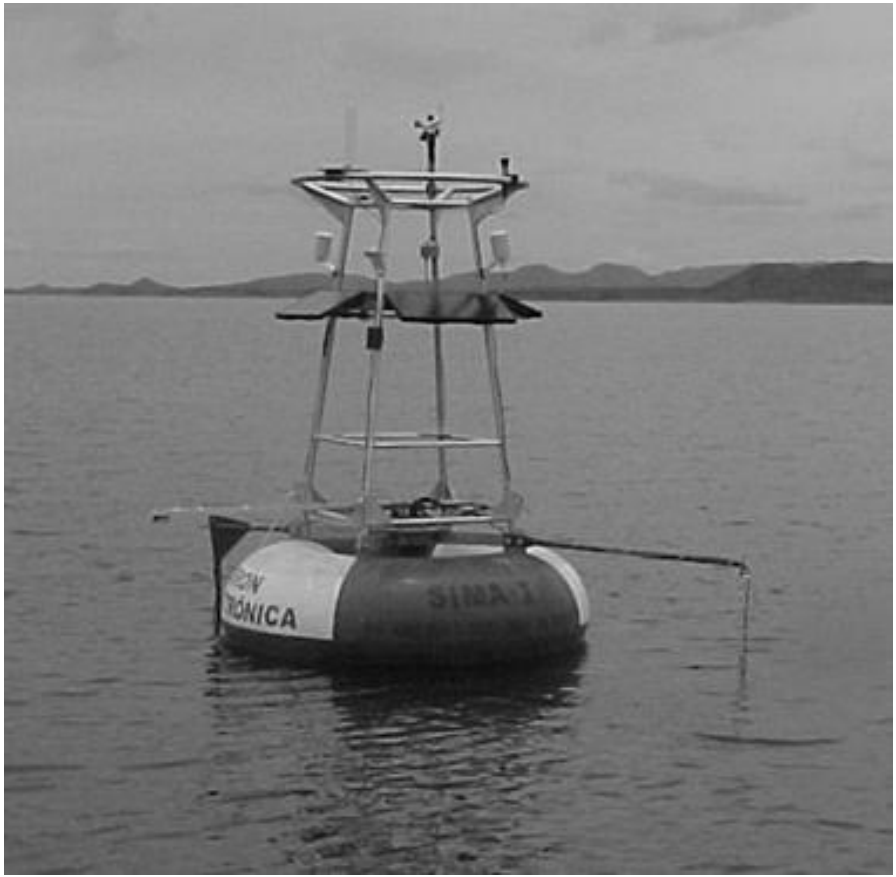


**Fig. 2.** Photo of the SIMA installed at Curuai floodplain (see Fig. 1 for location).





BGD
8, 3739–3770, 2011



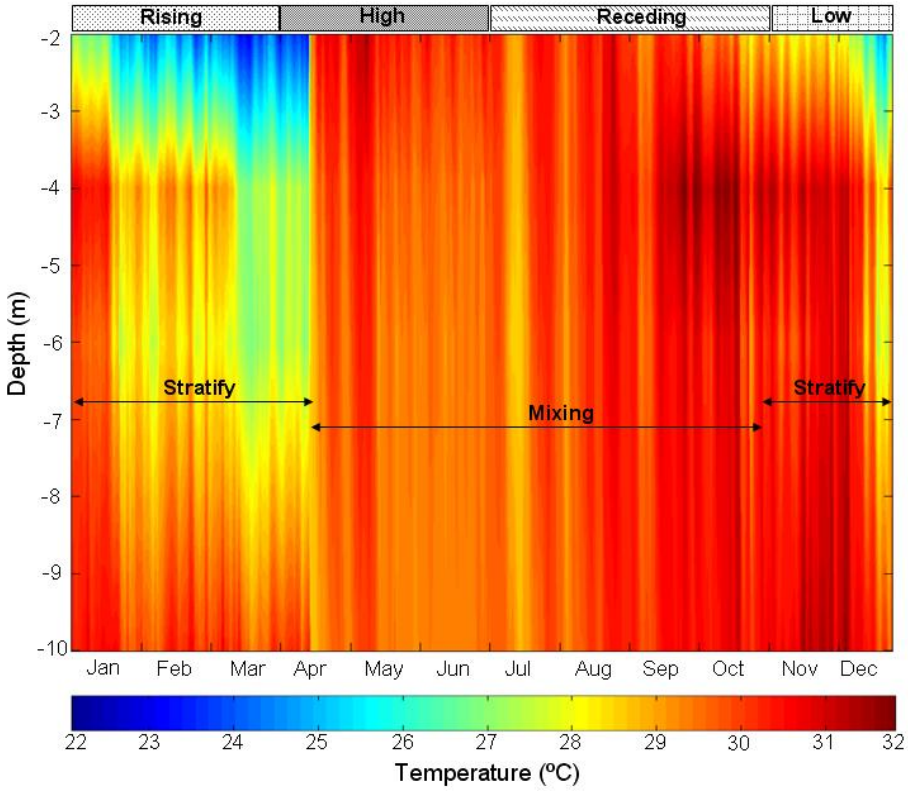


**Fig. 3.** Curuai floodplain thermal structure.





BGD
8, 3739–3770, 2011



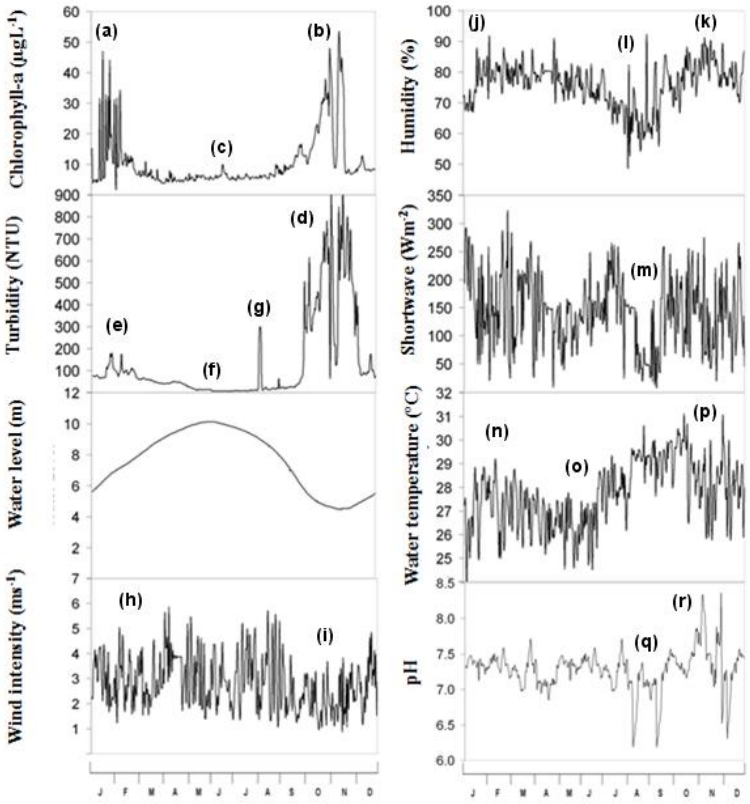


**Fig. 4.** Time series of limnological and meteorological variables measured by SIMA.





BGD
8, 3739–3770, 2011



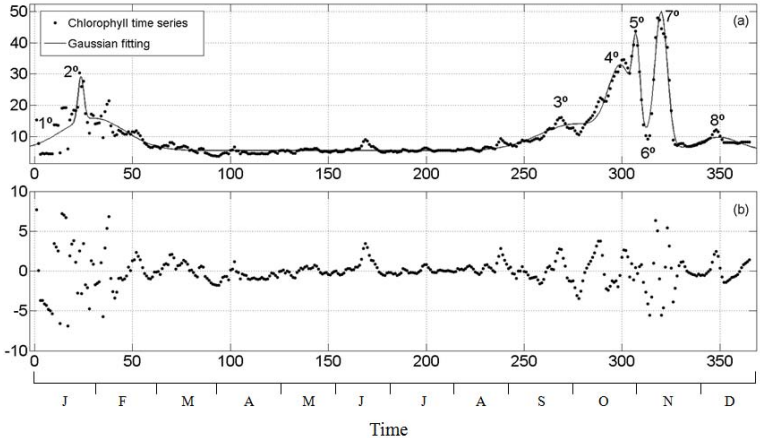


**Fig. 5.** Fitting the chlorophyll-*a* time series using eight-term Gaussian series.





BGD
8, 3739–3770, 2011



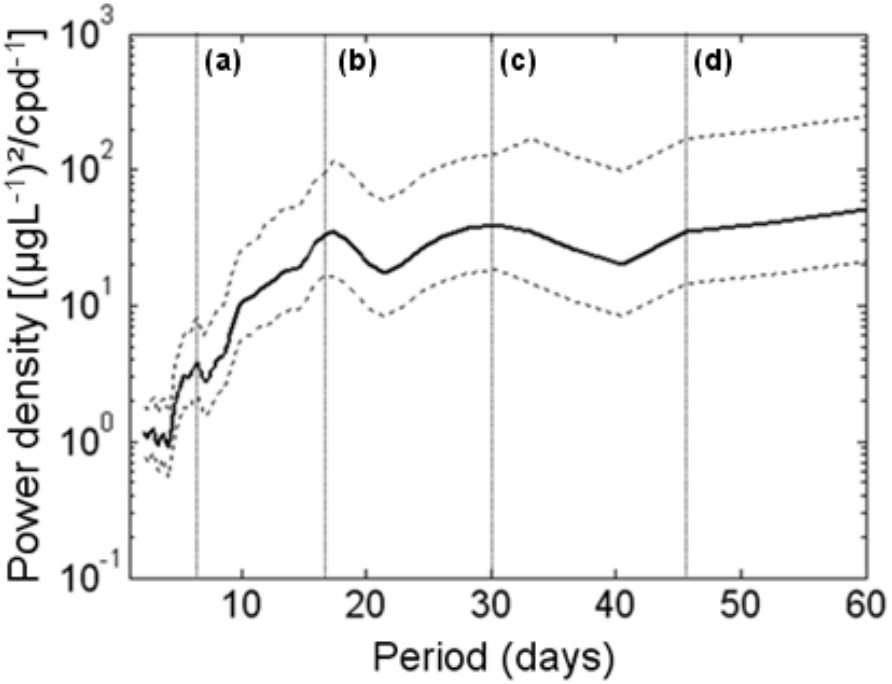


**Fig. 6.** Fourier power spectrum of chlorophyll-*a* time series. The dashed lines represent the confidence intervals limits.





BGD
8, 3739–3770, 2011



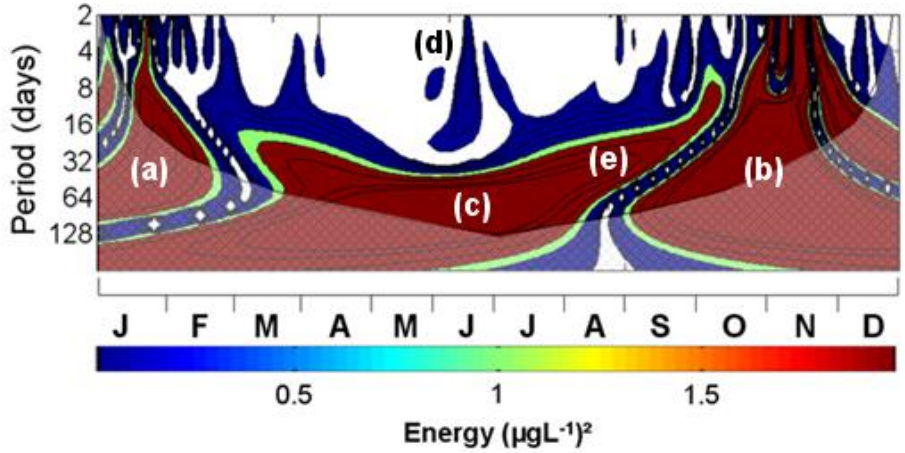


**Fig. 7.** Wavelet analysis of chlorophyll-*a* concentration time series. The line cross the power spectrum indicates the "cone of influence," where edge effects become important.





BGD
8, 3739–3770, 2011



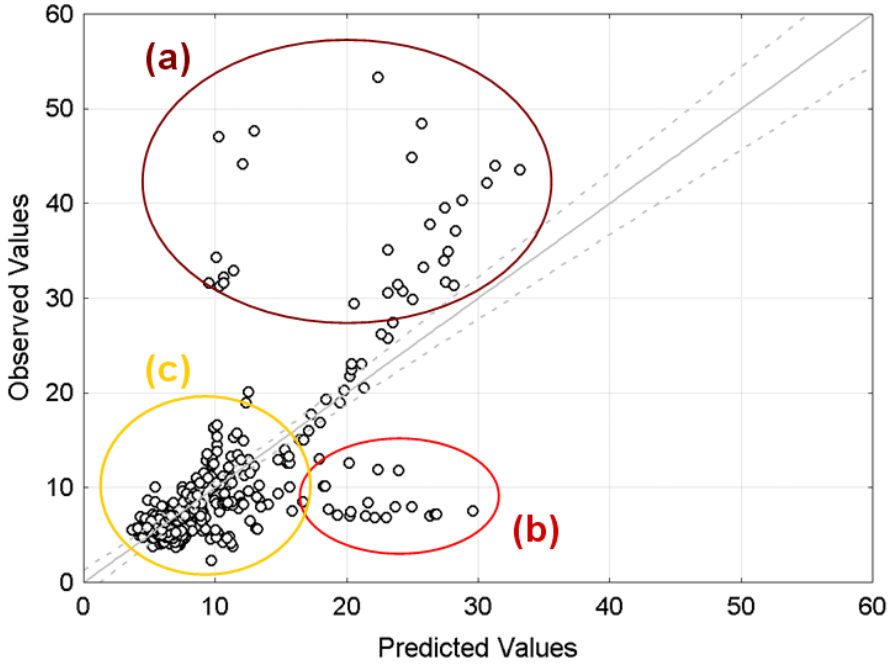


**Fig. 8.** Evaluation of the statistical model to estimate the chlorophyll-*a* concentration ($\mu g\,L^{-1}$) based on water level change and turbidity values.





BGD
8, 3739–3770, 2011



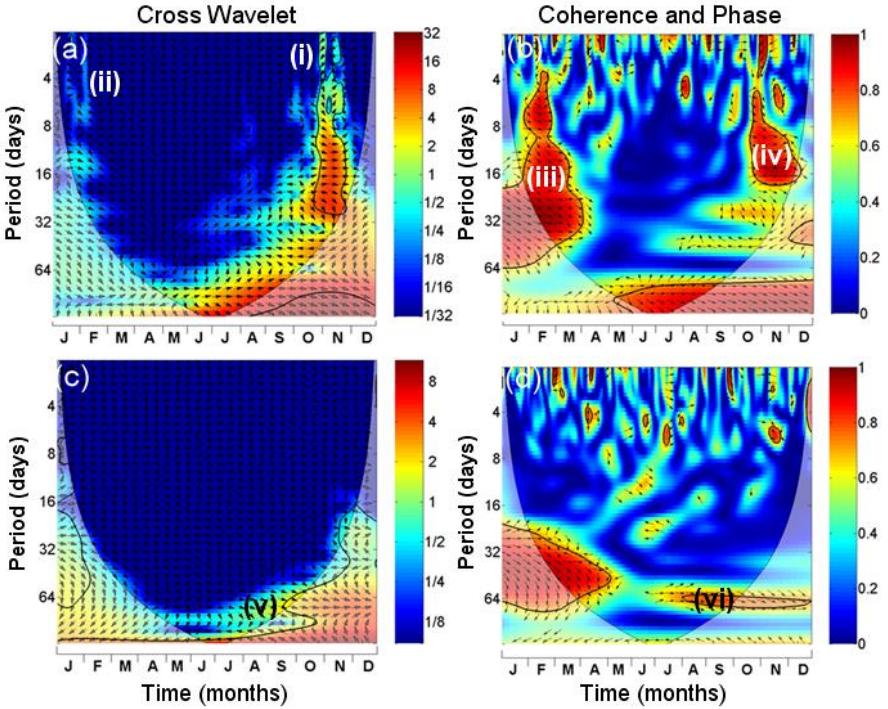


**Fig. 9.** Cross wavelet transform of the standardized chlorophyll against turbidity **(a)** and water level **(c)**. The 5% significance level against red noise is shown as a thick contour. The relative phase relationship is shown as arrows; squared wavelet coherence between the standardized chlorophyll and turbidity **(b)**, water level **(d)**. The 5% significance level against red noise is shown as a thick contour.





BGD
8, 3739–3770, 2011